An Evaluation of Ignition Criteria through State Classification and Detailed Simulation

Kevin P. Grogan, Matthias Ihme
Stanford University
Stanford, CA, USA

Submitted to the Special Session Convened by John Lee

1 Introduction

The stochastic development of discrete autoignition kernels within a combustible gas is known as weak ignition. In contrast to weak ignition, the strong ignition process is both uniform and regular; figure 1 shows simulations [6] of weak and strong ignition in a shock tube system. Strong ignition is generally the desired autoignition regime for chemical kinetic studies and homogeneous charge compression ignition (HCCI) engines. Weak ignition has been found in both shock tubes (ST) [1–6] and rapid compression machines (RCM) [7–10]. Furthermore, the notion of weak ignition has been extended to characterize the highly unstable and irregular nature of certain detonation waves [11]. Hence, the essential processes of weak ignition are posited to be inherent in many configurations.

The best features to classify these ignition varieties has been moot for over five decades [1, 2, 12, 13], and there is no current consensus on the most relevant features that predict the combustion mode. Meyer and Oppenheim [2] used the gradient in temperature of the ignition delay to demarcate the weak ignition regime. Subsequently, Sankaran *et al.* [13] delimited the weak ignition regime by comparing the laminar flame speed to the speed of the autoignition front. Additionally, Gu *et al.* [12] observed that the ignition variety depends on the thermoacoustic resonance of a hot spot. Furthermore, the SWACER mechanism of Lee *et al.* [14] has been used to describe reaction dynamics of an ignition kernel [6, 15].

Hence, it is the objective of this work to apply state classification to elucidate the most relevant features in predicting this phenomenon in STs, RCMs, and detonations using experimental data aggregated from the literature [2, 4, 5, 7, 9, 16, 17] and detailed simulation data [6]. Since these configurations are unique in their inherent fluid dynamics, this work will analyze the classification problem both separately and together to draw conclusions about the universality of the proposed features. From this, the relative importance of the examined features are measured and an interpretation of the prevalent physical processes is made. Finally, the evidence of existence of a universal governing parameter is investigated.

Correspondence to: kgrogan@stanford.edu

2 Methodology

In the simplest reduction of this work, it is a binary classification problem; that is, given a set of features, is the ignition variety strong or weak? For this, the following feature set is considered:

$$\mathcal{F} = \left\{ \frac{\tau_{\mathrm{IGN}}}{\tau_{\mathrm{E}}}, \frac{Q}{RT}, \Theta, \mathrm{Sa}, \xi, \mathrm{Pr}, \gamma, \mathrm{M}, \mathrm{Re} \right\} , \tag{1}$$

where the ignition delay and excitation times are denoted by τ_{IGN} and τ_{E}, respectively; Q is the amount of heat deposited during ignition; R and T are the universal gas constant and temperature, respectively; and the ignition sensitivity is given by $\Theta = \partial \ln \tau_{\mathrm{IGN}} / \partial \ln T$. The Sankaran number [13] compares the laminar flame speed of a mixture, S_{L}, to the speed of the reaction front, u_{RF}: $\mathrm{Sa} = \frac{S_{\mathrm{L}}}{u_{\mathrm{RF}}} = S_{\mathrm{L}} \frac{\partial \tau_{\mathrm{IGN}}}{\partial T} \frac{\partial T}{\partial x}$, where x is the direction of propagation for the reaction front, and the Zeldovich relation [18] is used for the speed of the reaction front is applied; furthermore, it is assumed that $\partial T / \partial x \propto T/L$, where L is the reference length scale (i.e., the bore diameter for STs and RCMs and the cellular length scale for detonations [19]); the flame speed is estimated using an analytical relation [20].

Similarly, the chemical resonance [12], ξ, compares the speed of sound in the mixture, a, to the speed of the reaction front: $\xi = a \frac{\partial \tau_{\mathrm{IGN}}}{\partial T} \frac{\partial T}{\partial x}$, where $\partial T / \partial x \propto T/L$ as with the Sankaran number.

Finally, the Prandtl number, specific heat ratio, Mach number, and Reynolds number are denoted by Pr, γ, M, and Re, respectively, and the convective speed, u, is used for the computation of the Mach and Reynolds number (i.e., the post-shock speed for the ST and detonation and the piston speed for the RCM). It also could indicate a covariance with a hidden feature not examined.

The logistic regression [21] is the linear classifier used for this work. The logistic regression is a discrete analog of the better known least-squares regression, and is used extensively for classification problems. Due to the self-similarity of the physical processes of ignition, the presented features are combined using a power law: $\eta = \prod_{i=1}^{|\mathcal{F}|} \chi_i^{w_i}$, where $\chi_i \in \mathcal{F}$, and η is the classification criterion (e.g., $\eta >$const. $\implies$ weak ignition). Defining ϕ_i as the natural log of χ_i, $\phi_i = \ln \chi_i$, a linear model is developed as $\beta = \ln \eta = w^{\top} \phi$, where w is the weight vector to be determined by the logistic regression. Since the natural log function is strictly monotonic, β can be used with the proposed linear classifier.

Additionally, the features are ranked using forward-stepwise selection [21]. Forward-stepwise selection is a greedy optimization algorithm, which selects features one-at-a-time to be used for the classification problem. More explicitly, in the first step of the algorithm, the set of all features are considered individually for the classification problem, and the single feature that yields the lowest test error is added to the feature set. The algorithm continues in this manner adding one feature at a time to the set while using the features previously added for the classification. What one obtains is an effective ranking of the most important features going from the first feature added to the last.

The data used in this work is summarized in Table 1. The ignition delay and excitation times are extracted from the data using the mechanisms provided in Table 1. Additionally, two detailed simulations of stoichiometric hydrogen/oxygen ignition in a shock tube [6] are utilized; these are shown in Fig. 1. Figure 1(a) shows a strong ignition event found in simulation while Fig. 1(b) shows a weak ignition event. The reacting simulations provide a comparison of the two different methodologies to predict: a data-driven approach, which makes extensive use of experimental data; and a first-principles high-fidelity simulation.

Table 1: Summary of the aggregated experimental data. The chemical mechanism used is cited in the Fuels column.

Author	Configuration	Fuels
Yamashita *et al.* [5]	ST	Acetylene *et al.* [22]
Penyazkov *et al.* [4]	ST	Propane [22]
Meyer and Oppenheim [2]	ST	Hydrogen [23]
Huang *et al.* [24]	ST	Methane [25]
Mansfield *et al.* [9]	RCM	Syngas [25]
Walton *et al.* [7]	RCM	Iso-Octane *et al.* [26]
Radulescu [17]	DET	Hydrogen [23], Methane [25], Acetylene [22], Ethylene [22], Propane [22]
Austin [16]	DET	Hydrogen [23], Ethylene [22], Propane [22]

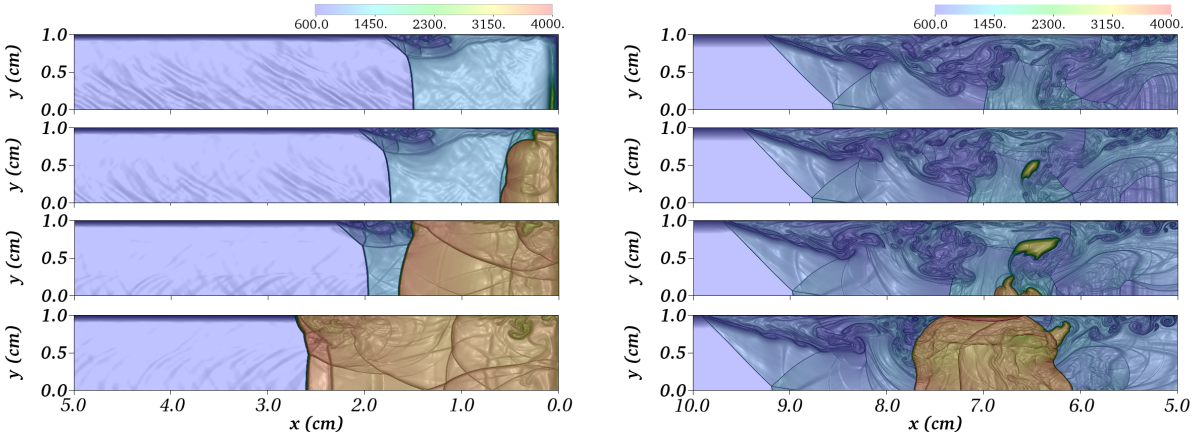

(a) Strong Ignition. $T = 1100$ K and $p = 3$ bar.

(b) Weak Ignition. $T = 1050$ K and $p = 3$ bar.

Figure 1: Evolution of the temperature field during the ignition process for two stoichiometric H_2/O_2 mixtures. Cases taken from [6]. The magnitude of the temperature gradients is overlaid.

3 Results

The results of the forward-stepwise selection algorithm are shown in Fig. 2. The left bars show the test error if each feature is added to the feature set. The test error is defined as

$$\epsilon_{\text{TEST}} = \frac{\sum_{i=1}^{|\mathcal{X}_{\text{TEST}}|} \mathbf{1}\left\{\hat{y}_i \neq y_i\right\}}{|\mathcal{X}_{\text{TEST}}|} \tag{2}$$

where $\mathbf{1}\{...\}$ is the indicator function and returns 1 if the statement is true and 0 otherwise, $\hat{y}_i$ is the label predicted by the regression (i.e., weak or strong), and y_i is the known label. The test set is separated from the data set used for the regression to reduce model bias.

The right error bars shows how the test error of the given feature compares to the test error when the other remaining features are added. This metric seeks to clarify how much better the added feature is to the remaining features; that is, a value near 1 indicates that the selected feature is not much better than the remaining features, and the algorithm is essentially randomly selecting features.

The large error bars in the detonation data set is attributed to the sparsity of the data compared to the other configurations. As shown in the figure, features involving the combustion time scales and sensitivity prove

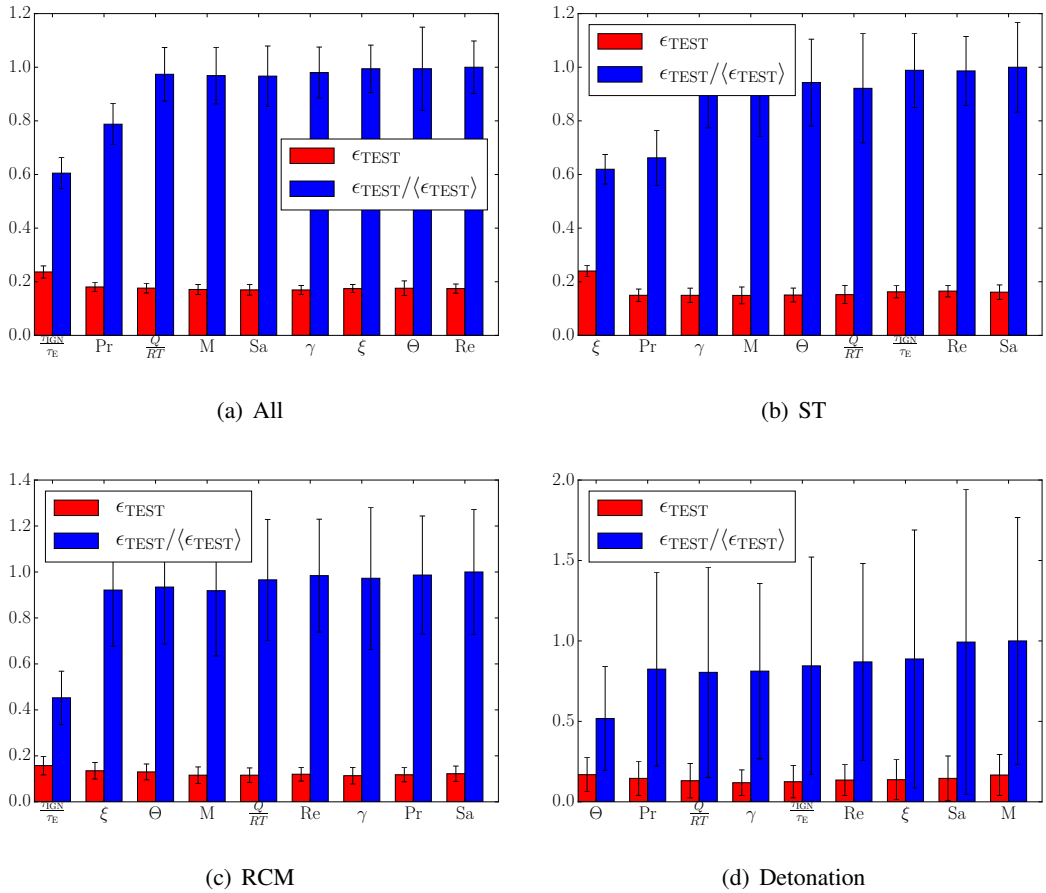

(a) All (b) ST

(c) RCM (d) Detonation

Figure 2: Results of the forward-stepwise selection of features. Features are selected in order going from left to right. The mean test error, $\langle\epsilon_{\mathrm{TEST}}\rangle$, is the mean of all the test errors produced when each feature that is not currently in the set is added. The error bars are determined by bootstrapping the data set to determine the variance in the test error.

to be the most efficacious (i.e., $\tau_{\mathrm{IGN}}/\tau_E$, ξ, and Θ), and are selected by the algorithm first; this indicates that the ignition phenomena is most strongly influenced by the chemical time scales; it also indicates that necessary gasdynamic perturbations are not well-captured with given features.

Additionally, it is shown that the Prandtl number significantly influences the classifier for all configurations except the RCM; it is noted that the RCM only needs the feature $\tau_{\mathrm{IGN}}/\tau_E$ to classify the ignition regime. The significance of the Prandtl number may indicate that the competition between viscous and thermal diffusion plays an important role.

Furthermore, the figure demonstrates that at most two non-dimensional groups are sufficient to classify the ignition variety using the proposed power-law model. This gives credence to the possibility of a universal governing parameter.

Additionally, upon further inspection of the ranking of features produced at each step of the algorithm, a clear preference for ξ over Sa arises indicating that the speed of sound is a more substantial velocity scale

than the laminar flame speed; this implies that the thermoacoustic feedback of the SWACER mechanism may play a substantial role given the interpretation of these numbers.

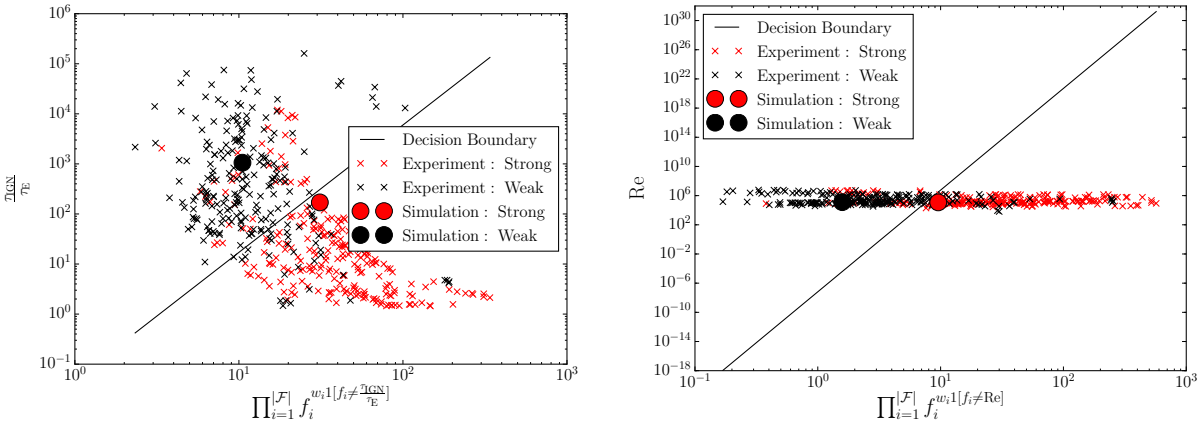

(a) (b)

Figure 3: Plot of the decision boundaries created for two selected features. The entire feature and data set is used.

The decision boundaries produced by the logistic regression classifier for two selected features are shown in Fig. 3. The chemical time scale ratio, $\tau_{\mathrm{IGN}}/\tau_{\mathrm{E}}$, and the Reynolds numbers, Re, are shown since the forward-stepwise selection algorithm selected these two features to be the most and least effective, respectively. It is shown that the slope of the decision boundary in Fig. 3(a) is quite shallow indicating that a small change in the chemical time scale ratio could produce a change in classification. For the Reynolds, the opposite is true. Fig. 3(b) shows that a rather substantial change in the Reynolds number is necessary to produce a change in the classification; more precisely, the ordinate of Fig. 3(b) 48 orders of magnitude while Fig. 3(a) spans only 7 with the abscissa being relatively similar in both cases.

From Fig. 3(a), it is apparent that the data is not linearly separable; while significant clustering is demonstrated for the chemical time scale ratio, excursions deep into the strong and weak regimes are shown. This is indicative that the power-law model is insufficient to classify all the data; a more advanced model such as an artificial neural network could produce superior results. However, it is argued that the simple linear model captures most of the sensitivities and that the majority of the data respects the given boundary.

Additionally, the detailed simulations correspond to the classifier's predictions; the strong ignition case is shown to be close to the decision boundary, and some inhomogeneous characteristics are demonstrated in Fig. 1(a). Finally, weak ignition is shown to occur for large values of the chemical timescale ratio as expected from the theory.

4 Conclusions

The best features to classify the weak ignition regime is a current topic of interest in the combustion community. This work used state classification techniques to investigate several proposed features and to tease out sensitivities via a data-driven approach. From this, it was found that the features that represent the

combustion timescale and sensitivity performed the best for all configurations examined; however, features which better incorporate gasdynamic fluctuations are necessary for a complete characterization. Finally, no significant improvement was found in the test error for more than two features, which suggests that the correct classification of the combustion process is low-dimensional and that a universal governing parameter is plausible.

5 Acknowledgments

The authors gratefully acknowledge financial support through the Air Force Office of Scientific Research under Award No. FA9550-14-1-0219.

References

[1] V. V. Voevodsky and R. I. Soloukhin. On the mechanism and explosion limits of hydrogen-oxygen chain self-ignition in shock waves. *Proc. Combust. Inst.*, 10:279–283, 1965.

[2] J. W. Meyer and A. K. Oppenheim. On the shock-induced ignition of explosive gases. *Proc. Combust. Inst.*, 13:1153–1164, 1971.

[3] D. J. Vermeer, J. W. Meyer, and A. K. Oppenheim. Auto-ignition of hydrocarbons behind reflected shock waves. *Combust. Flame*, 18:327–336, 1972.

[4] O. Penyazkov, K. Ragotner, A. Dean, and B. Varatharajan. Autoignition of propane-air mixtures behind reflected shock waves. *Proc. Combust. Inst.*, 30:1941–1947, 2005.

[5] H. Yamashita, J. Kasahara, Y. Sugiyama, and A. Matsuo. Visualization study of ignition modes behind bifurcated-reflected shock waves. *Combust. Flame*, 159:2954–2966, 2012.

[6] K. P. Grogan and M. Ihme. Weak and strong ignition of hydrogen/oxygen mixtures in shock-tube systems. *Proc. Combust. Inst.*, 35(2):2181–2189, 2015.

[7] S. M. Walton, X. He, B. T. Zigler, M. S. Wooldridge, and A. Atreya. An experimental investigation of iso-octane ignition phenomena. *Combust. Flame*, 150:246–262, 2007.

[8] S. M. Walton, X. He, B. T. Zigler, and M. S. Wooldridge. An experimental investigation of the ignition properties of hydrogen and carbon monoxide mixtures for syngas turbine applications. *Proc. Combust. Inst.*, 31:3147–3154, 2007.

[9] A. Mansfield and M. S. Wooldridge. High-pressure low-temperature ignition behavior of syngas mixtures. *Combust. Flame*, 161:2242–2251, 2014.

[10] K. P. Grogan, S. S. Goldsborough, and M. Ihme. Ignition regimes in rapid compression machines. *Combust. Flame*, 162(8):3071–3080, 2015.

[11] M. I. Radulescu, G. J. Sharpe, and D. Bradley. A universal parameter quantifying explosion hazards, detonability and hot spot formation: the χ number. *Proc. of the Seventh International Seminar on Fire and Explosion Hazards*, 7, 2013.

[12] X. Gu, D. Emerson, and D. Bradley. Modes of reaction front propagation from hot spots. *Combust. Flame*, 133:63–74, 2003.

[13] R. Sankaran, H. G. Im, E. R. Hawkes, and J. H. Chen. The effects of non-uniform temperature distribution on the ignition of a lean homogeneous hydrogen–air mixture. *Proc. Combust. Inst.*, 30:875–882, 2015.

[14] J. H. Lee, R. Knystautas, and N. Yoshikawa. Photochemical initiation of gaseous detonations. *Acta Astronautica*, 5:971–982, 1978.

[15] Y. Lv and M. Ihme. Computational analysis of re-ignition and re-initiation mechanisms of quenched detonation waves behind a backward facing step. *Proceedings of the Combustion Institute*, page submitted, 2014.

[16] J. M. Austin. *The Role of Instability in Gaseous Detonation*. PhD thesis, California Institute of Technology, 2003.

[17] M. I. Radulescu. *The propagation and failure mechanism of gaseous detonations: Experiments in porous-walled tubes*. PhD thesis, McGill University, 2003.

[18] Y. B. Zeldovich. Regime classification of an exothermic reaction with nonuniform initial conditions. *Combust. Flame*, 39:211–214, 1980.

[19] J. H. S. Lee. *The Detonation Phenomenon*. Cambridge University Press, Cambridge, 2008.

[20] S. R. Turns. *An Introduction to Combustion: Concepts and Applications*. McGraw Hill, 2000.

[21] T. Hastie, R. Tibshirani, and J. Friedman. *The Elements of Statistical Learning*. Springer, 2nd edition, 2008.

[22] D. Healy, H. J. Curran, S. Dooley, J. M. Simmie, D. M. Kalitan, E. L. Petersen, and G. Bourque. Methane/propane mixture oxidation at high pressures and at high, intermediate and low temperatures. *Combust. Flame*, 155(3):451–461, 2008.

[23] Z. Hong, D. Davidson, and R. Hanson. An improved H_2/O_2 mechanism based on recent shock tube/laser absorption measurements. *Combust. Flame*, 158:633–644, 2011.

[24] J. Huang, P.G. Hill, W.K. Bushe, and S.R. Munshi. Shock-tube study of methane ignition under engine-relevant conditions: experiments and modeling. *Combust. Flame*, 136:25–42, 2004.

[25] J. Li, Z. Zhao, A. Kazakov, M. Chaos, F. L. Dryer, and J.J. Scire, Jr. A comprehensive kinetic mechanism for CO, CH_2O, and CH_3OH combustion. *Int. J. Chem. Kinet.*, 39:109–136, 2007.

[26] M. Mehl, W. J. Pitz, C. K. Westbrook, and H. J. Curran. Kinetic modeling of gasoline surrogate components and mixtures under engine conditions. *Proc. Combust. Inst.*, 33:193–200, 2011.